Random sequential adsorption of anisotropic particles. I. Jamming limit and asymptotic behavior

P. Viot and G. Tarjus
Laboratoire de Physique Théorique des Liquides,[a] *Université Pierre et Marie Curie, 4, place Jussieu 75252 Paris Cedex 05 France*

S. M. Ricci and J. Talbot
School of Chemical Engineering, Purdue University West Lafayette, Indiana 47907

(Received 14 April 1992; accepted 22 June 1992)

We study the random sequential adsorption (RSA) of unoriented anisotropic objects onto a flat uniform surface, for various shapes (spherocylinders, ellipses, rectangles, and needles) and elongations. The asymptotic approach to the jamming limit is shown to follow the expected algebraic behavior, $\theta(\infty)-\theta(t)\sim t^{-1/3}$, where θ is the surface coverage; this result is valid for all shapes and elongations, provided the objects have a nonzero proper area. In the limit of very small elongations, the long-time behavior consists of two successive critical regimes: The first is characterized by Feder's law, $t^{-1/2}$, and the second by the $t^{-1/3}$ law; the crossover occurs at a time that scales as $\epsilon^{-1/2}$ when $\epsilon\to 0$, where ϵ is a parameter of anisotropy. The influence of shape and elongation on the saturation coverage $\theta(\infty)$ is also discussed. Finally, for very elongated objects, we derive from scaling arguments that when the aspect ratio α of the objects becomes infinite, $\theta(\infty)$ goes to zero according to a power law α^{-p}, where $p=1/(1+2\sqrt{2})$. The fractal dimension of the system of adsorbed needles is also discussed.

I. INTRODUCTION

A variety of large molecules, specifically proteins and latex particles, have been shown to adsorb in an essentially *irreversible* manner.[1-5] Rates of both desorption and surface diffusion are very slow compared to the rate of adsorption. In the many cases where particles do not adsorb on top of each other and thus form only monolayers, it has been suggested that the random sequential adsorption (RSA) model may be appropriate.[1] RSA is a process in which objects are placed at random on a surface such that they do not overlap with any that have already been successfully placed. Once on the surface, the position of an object remains permanently fixed, which ensures the irreversible character of the adsorption process. Initially, the probability of placing a new object is high and the surface fills rapidly. As the surface coverage increases, the adsorption probability decreases due to exclusion effects from preadsorbed objects until, eventually, it is impossible to place another object without overlap. This condition, associated with a zero probability of adsorption, is commonly known as the jamming limit. For a RSA on a continuous uniform surface, the approach to the jamming limit is characterized by an algebraic, as opposed to an exponential, time dependence.

Until recently, nearly all of the published work on RSA has focused on spherical particles. This is clearly a limitation since many of the substances studied are in fact nonspherical. For example, the human plasma protein fibrinogen is often modeled in adsorption experiments as a rod of aspect ratio 7.5:1.[3] As, moreover, there is a range of bulk concentrations for which such proteins adsorb exclusively "side-on",[3] it seems relevant to investigate the RSA process of two-dimensional anisotropic particles deposited onto a uniform surface. This case is more complex than the RSA of hard disks, as can be understood by considering the rate equation governing the time evolution of the surface coverage $\theta(t)$: this equation takes the form of a "generalized Langmuir equation,"

$$\frac{d\theta}{dt}=k_a\int d\Omega\, f(\Omega)\Phi[\theta(t),\Omega], \tag{1}$$

where k_a is the "bare" rate of adsorption (which is set equal to 1 in the following without loss of generality), $f(\Omega)$ is the probability distribution for the orientations Ω of the incoming particles [we restrict ourselves to the consideration of a uniform distribution $f(\Omega)=1/2\pi$], and $\Phi[\theta(t),\Omega]$ represents the probability of adding a new particle with an orientation Ω when the surface coverage is equal to θ. $\Phi[\theta(t),\Omega]$ can also be interpreted as the fraction of the total surface that is available to the center of a new particle with an orientation Ω; we call it the available surface function (ASF). The fact that the ASF is orientation dependent changes the main features of the RSA (saturation coverage, asymptotic kinetics, structure of the monolayer, etc.), when compared to the hard-disk case.

By formally integrating Eq. (1), one can deduce the coverage as a function of time. However, except for the standard one-dimensional car parking problem,[6-8] the ASF is not exactly determined, which requires the extensive use of the computer simulation. For descriptive purposes it is fruitful to divide the RSA kinetics into several "regimes":[9] a low-to-moderate coverage regime, for which coverage and time expansions can be developed,[7,9-14] and a high-coverage regime which corresponds to the asymptotic ap-

[a]Unité de Recherche Associée au CNRS. (URA 765).

 0021-9606/92/195212-07$006.00

proach towards the jamming limit (the ASF goes to zero and consists of very small disconnected areas) and for which exact results can be derived.[15–19] As will be discussed in Sec. IV, an additional "intermediate" regime must be introduced when considering the RSA of very elongated objects. In this paper, we focus on the asymptotic and intermediate regimes as well as on the dependence of the saturation coverage upon particle shape and elongation. The second paper is devoted to the low-to-moderate-coverage regime and to the validity of various approximate interpolation formulas devised for describing the full range of coverages. A forthcoming third paper will consider the structure of the RSA configurations of anisotropic objects and their comparison with the corresponding equilibrium configurations.

The present paper is organized as follows. In Sec. II, we detail the simulation procedures and data analysis. The results for the asymptotic kinetics and saturation coverage are given in Sec. III. By careful examination of various shapes (rectangles, ellipses, spherocylinders, or more precisely discorectangles) and elongations, we confirm that the coverage approaches its saturation value with an algebraic time dependence, the exponent of which is equal to 1/3. For weakly elongated ellipses and spherocylinders, the asymptotic regime can be divided into two regions: The first is characterized by Feder's law, $t^{-1/2}$, and the second by the $t^{-1/3}$ law; the time of the crossover is shown to increase as $\epsilon^{-1/2}$ when $\epsilon \to 0$, where ϵ is a parameter of anisotropy that vanishes in the limit of disks. In addition, we discuss the influence of shape and elongation on the efficiency of the filling process. Finally, in Sec. IV, we study the limit of very elongated objects. By scaling arguments, we show that when the aspect ratio α is very large, the saturation coverage goes to zero according to a power law, $\theta_\alpha(\infty) \sim \alpha^{-p}$, where $p = 1/(1+2\sqrt{2})$. This result is obtained by introducing an intermediate regime in which the filling by very elongated objects is insensitive to the width (or smallest linear size) of the objects and is thus similar to the filling by infinitely thin needles, a process which has been recently studied.[20–23] The characteristic time for the crossover between the intermediate and asymptotic regimes is shown to scale as $\alpha^{3/(1+2\sqrt{2})}$. Following the arguments given in Ref. 22, we find that the fractal dimension of the system of adsorbed needles is equal to $(1+4\sqrt{2})/(1+2\sqrt{2})$.

II. SIMULATION PROCEDURES AND DATA ANALYSIS

We consider the RSA of several kinds of two-dimensional hard convex bodies (rectangles, ellipses, spherocylinders, needles) with various aspect ratios, $\alpha \geqslant 1$: α is defined as the ratio of the long axis a to the short axis b for ellipses and spherocylinders (discorectangles in 2D), as the ratio of the length L to the width l for rectangles, and is infinite for needles. When $\alpha \to 1$, spherocylinders and ellipses reduce to the isotropic case, i.e., disks, whereas rectangles reduce to an anisotropic case, i.e., squares. The simulation procedures are as follows. Each run starts with an empty square cell with periodic boundary conditions. At each step, a trial object is sampled with random position and orientation that are both chosen from uniform probability distributions. In order to reduce the number of tests for overlap between the trial object and objects that are already placed, a systematic grid construction is adopted. For ellipses, squares, and rectangles, the procedures for overlap tests have been described previously.[18,19,24] For spherocylinders, noting that they can be thought of as a locus of points equidistant from a line segment in a plane, the overlap test amounts to determining the minimum distance between two line segments: overlap occurs when the distance is less than b.

When the aspect ratio α increases, three cumulative effects reduce the efficiency of the simulations: (1) finite-size effects grow as the ratio of largest linear size of the object over the linear size of the square cell; (2) Even with the grid construction, the region which is accessible to a trial object goes up as α^2 and the number of tests increases accordingly; (3) As discussed in Sec. IV, the characteristic time of the beginning of the asymptotic behavior grows with α. In simulations, we set the system size s (defined as the ratio of the proper area of one object to the area of the square cell) equal to 0.002 for ellipses, and 0.0002 for spherocylinders and rectangles with an aspect ratio α between 1 and 15. For needles, which have no proper area, the ratio of the needle length over the length of the cell side was taken as 0.05. Since some simulation data have been already published in the literature for ellipses,[18,20] squares,[19,24] rectangles,[21,24] and needles,[20–22] but not for spherocylinders, we have paid special attention to the spherocylinder simulations in order to minimize all possible sources of error and uncertainty: the simulations for every aspect ratio include from 500 to 750 independent runs, each consisting of 10^8 trials, and an accelerating procedure, described briefly as follows, was used. The spherocylinder simulations also make use of a systematic grid construction such that only one particle can lie within a grid element. The specific new feature is the identification of those grid elements which cannot accept the center of a new particle in any orientation. The random number generator is then applied only to those grid elements that have not been so identified and the number of adsorption attempts is scaled appropriately. Thus if a fraction f of the surface has been discounted, each adsorption attempt corresponds to $1/(1-f)$ attempts of a conventional algorithm.

In order to discount a grid element, one must check that every point within it is inaccessible to a new particle in any orientation. Practically, this requires that the surface be discretized. We used a fine-mesh lattice with a density of points sufficient to approximate a continuous surface. In the simulations reported here, each grid contained 625 points. The procedure for testing the availability of a discrete point within a grid is a rather involved geometrical problem. A full discussion of the method, together with other simulation details, will be presented elsewhere.

The asymptotic regime of the process is characterized by the fact the ASF consists mostly of small isolated targets in which only one additional particle can be inserted. The filling process is then very slow, with many attempts

TABLE I. Power law exponents p_α and saturation coverage $\theta_\alpha(\infty)$ characterizing the asymptotic regime of spherocylinders. The results were obtained from the simulation data by least-square fit procedures based on Eq. (2) (Ref. 19). R is the number of independent runs.

	Spherocylinders		
α	p_α	$\theta_\alpha(\infty)$	R
1.25	0.421±0.006	0.569±0.001	750
1.5	0.334±0.006	0.580±0.001	750
1.75	0.335±0.006	0.583±0.001	750
2	0.338±0.006	0.581±0.001	650
2.5	0.339±0.006	0.577±0.001	750
3	0.335±0.006	0.569±0.001	650
4	0.337±0.006	0.554±0.001	650
6	0.337±0.006	0.524±0.001	700
10	0.330±0.006	0.482±0.001	750
15	0.334±0.007	0.445±0.001	500

being required to add each new particle. The rarity of the successful events makes the study of the asymptotic kinetics rather difficult and raises some methodological questions which have been discussed by Viot and Tarjus.[19] We have analyzed the simulation data by looking for an asymptotic behavior of the following form:

$$\theta(t) \sim \theta_\alpha(\infty) - \frac{b_\alpha}{t^{p_\alpha}}, \tag{2}$$

where $\theta_\alpha(\infty)$, b_α, p_α are considered as *a priori* unknown and may depend upon the aspect ratio α. More details are given in Ref. 19, as well as in Tables I–III.

III. ASYMPTOTIC KINETICS AND SATURATION COVERAGE

Except for the case of weakly elongated ellipses and spherocylinders ($\alpha=1.25$), the power law exponents determined by using Eq. (2) (or its time derivative) were all found to be equal to 1/3, within statistical uncertainties (cf. Tables I–III). This confirms the result obtained first by Talbot *et al.*[18] and later by others.[19–21] It shows that, provided the anisotropic objects are inserted with random orientations, *shape and elongation do not influence the value of the power law exponent.* As will be discussed later on, this conclusion should also apply to weakly elongated ellipses and spherocylinders. The exponent seems to be simply given by the inverse of the number of degrees of freedom per object,[19] a result that can be rationalized by following the arguments given by Talbot *et al.*:[18] The asymptotic kinetics can be determined by studying the filling of small isolated targets, each target being characterized by a small length scale parameter h. For every degree of freedom (here two coordinates for the position of the center and one angle for the orientation), there is only a restricted range of values for which an object can reach a given target, provided the target is small enough, and the width of this range is proportional to h. Since all degrees of freedom must lie simultaneously within their respective range for an object to be successfully inserted in the given target, the rate $k(h)$ at which targets characterized by h disappear goes as $h^{\mathcal{N}}$, where $\mathcal{N}$ is the number of degrees of freedom per object (here, $\mathcal{N}=3$). The following rate equation can be written:

$$\frac{d}{dt} n(h,t) \sim -k(h) n(h,t) \sim -h^{\mathcal{N}} n(h,t), \quad t \to +\infty, \tag{3}$$

where $n(h,t)$ is the number density of h targets, so that the asymptotic equation for the time evolution of the coverage is

$$\theta(\infty) - \theta(t) \sim \int_0^{H_c} dh\, n(h,t) \sim t^{-1/\mathcal{N}}, \quad t \to +\infty, \tag{4}$$

where H_c is an (irrelevant) upper cutoff. Equation (4) expresses the fact that the number of targets at time t is equal to the number of particles that can still be inserted, and that only vanishingly small values of h are relevant to determine the asymptotic behavior. Note that the preceding reasoning is not valid when some of the degrees of freedom are chosen from a discrete probability distribution (e.g., for parallel nonspherical objects[16,25]) and for objects with no proper area (e.g., for infinitely thin needles[23] or mixtures with pointlike particles[26,27]).

We consider now the asymptotic regime of weakly elongated objects. For small elongations, following once again the treatment of Talbot *et al.*,[18] one can define two classes of targets: nonselective and selective. A target is nonselective if an object placed in this target can be freely rotated by 2π with only a slight displacement of its center; the rotation of 2π of the object requires that a roughly circular region of diameter d (where d is the *longest* length of the object) is free of neighboring objects [see Figs. 1(a) and 1(c)]. A selective target, on the other hand, is such that it is only for a limited range of orientations that a region of length d (and width $\geqslant b,l$) is free of objects [see Figs. 1(b) and 1(d)]. The selective targets are those which have been previously considered in deriving Eqs. (3) and (4). Since h is the length scale characteristic of the avail-

TABLE II. Same as Table I for ellipses.

	Ellipses		
α	p_α	$\theta_\alpha(\infty)$	R
1.25	0.43±0.05	0.568±0.001	200
1.5	0.33±0.03	0.580±0.001	200
2	0.32±0.03	0.583±0.001	200
3	0.32±0.03	0.569±0.001	200
4	0.32±0.03	0.552±0.001	200
5	0.35±0.03	0.536±0.001	200

TABLE III. Same as Table I for rectangles.

	Rectangles		
α	p_α	$\theta_\alpha(\infty)$	R
1	0.34±0.01	0.530±0.001	35
1.5	0.34±0.02	0.552±0.002	40
1.618	0.32±0.02	0.553±0.002	40
2	0.34±0.04	0.548±0.002	35
5	0.33±0.04	0.510±0.005	35
15	0.32±0.04	0.483±0.005	35

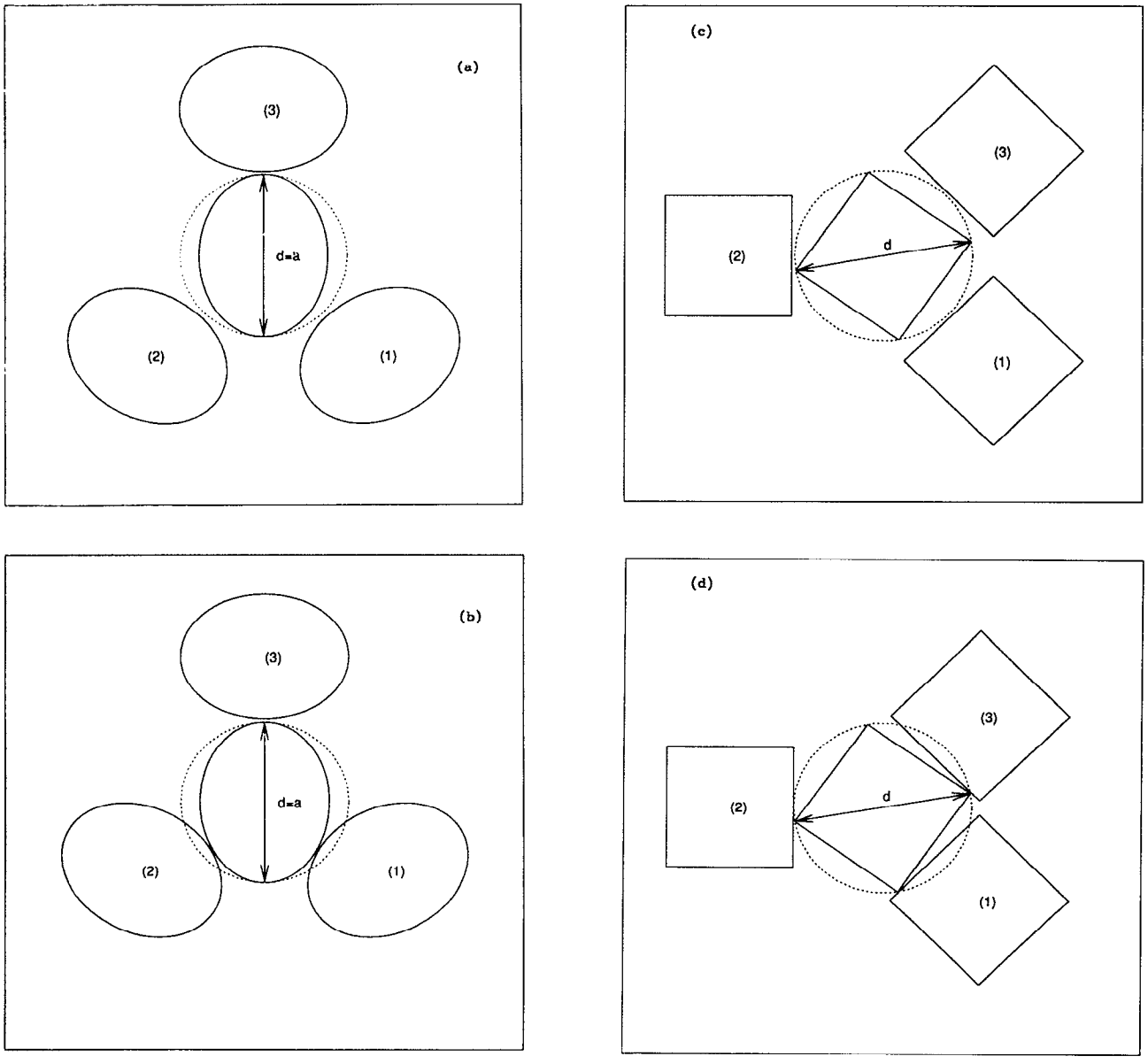

FIG. 1. Illustration of nonselective and selective targets for weakly elongated ellipses [(a) and (b), respectively] and rectangles [(c) and (d), respectively]. The targets are defined by three preadsorbed particles denoted (1), (2), and (3). For nonselective targets [(a) and (c)], one can rotate by 2π the test particle inserted in the middle: a circular region of diameter $d=a$ for ellipses (a) or $d=\sqrt{L^2+l^2}$ for rectangles (c) must be free of preadsorbed particles. For selective targets [(b) and (d)], one cannot rotate the test particle by 2π: only a limited range of orientations is allowed.

able space for the center of a new object, one concludes that for $h \geqslant (a-b)$ or $(d-l)$, the targets are selective and for $h \leqslant (a-b)$ or $(d-l)$, the targets are nonselective. The relevant anisotropy parameter is thus $\epsilon = a/b - 1 = \alpha - 1$ for ellipses and spherocylinders and $\epsilon = d/l - 1 = \sqrt{1+\alpha^2} - 1$ for rectangles. If one chooses b or l as unit length ($b \equiv 1$ or $l \equiv 1$), the switching from a selective to a nonselective target occurs for a length scale $h \sim \epsilon$. The leading term of the rate of disappearance for selective targets is $Ah^2(h/\epsilon)$, where (h/ϵ) is the range of allowed orientations; the rate for nonselective targets goes as $B(h-\epsilon)^2$ if h is large enough compared to ϵ. For small ϵ's, these features can be incorporated in the following ansatz:

$$k(h) = Ah^3/\epsilon, \quad h \leqslant \epsilon,$$
$$= A\epsilon^2 + B(h-\epsilon)^2, \quad h \geqslant \epsilon. \tag{5}$$

The evolution of the coverage $\theta_\epsilon(t)$ towards its saturation value is given by

$$\theta_\epsilon(\infty) - \theta_\epsilon(t) \sim \int_0^{H_c} dh\, n(h,t)$$
$$\sim \int_0^{\epsilon} n(h,t_c) e^{-Ah^3/\epsilon(t-t_c)}$$
$$+ \int_\epsilon^{H_c} n(h,t_c) e^{[A\epsilon^2 + B(h-\epsilon)^2](t-t_c)}, \tag{6}$$

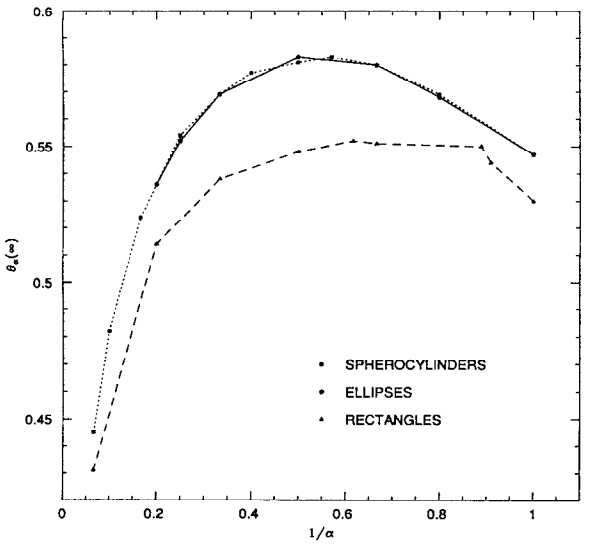

FIG. 2. Saturation coverage, $\theta_\alpha(\infty)$, as a function of the inverse of the aspect ratio α (for $1 \leqslant \alpha \leqslant 15$). The data points correspond to the results given in Tables I–III and in Refs. 18, 20, and 24. The lines are drawn for visual guidance.

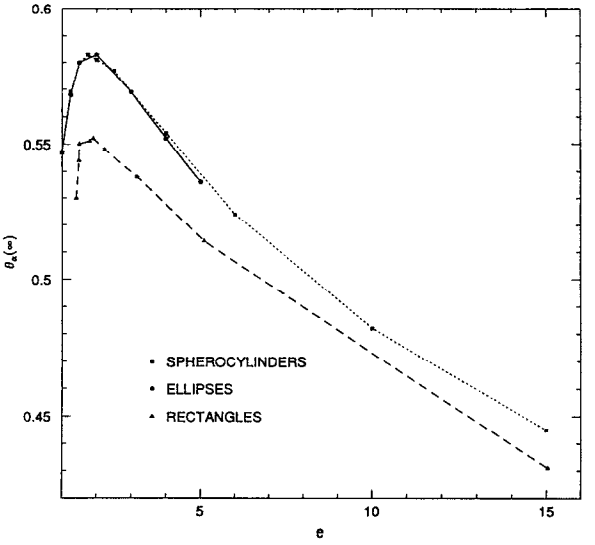

FIG. 3. Saturation coverage, $\theta(\infty)$, as a function of the elongation e defined in text ($e=\alpha$ for ellipses and spherocylinders, $e=\sqrt{1+\alpha^2}$ for rectangles). Other captions are same as in Fig. 2.

where t_c is the time at which the asymptotic regime starts. After some manipulations, one obtains

$$\theta_\epsilon(\infty)-\theta_\epsilon(t)\sim\epsilon\left\{\frac{\int_0^z dx\, e^{-x^3}}{z^{1/3}}+C\frac{e^{-z}}{z^{1/2}}\right\}, \quad t\to+\infty, \tag{7}$$

where $z=\epsilon^2 t$, $\epsilon \ll 1$, and $C>0$. It is now easy to expand Eq. (7) in the two limits $z \ll 1$ and $z \gg 1$, and we derive the following results: (i) the asymptotic regime is made of two successive regions, the first characterized by a $t^{-1/2}$ behavior and a second by a $t^{-1/3}$ behavior; the characteristic time of the crossover between the two behaviors is obtained for $z\sim 1$ and goes as $\epsilon^{-1/2}$. (ii) The $t^{-1/3}$ regime shrinks when $\epsilon\to 0$ and eventually vanishes (hard-disk case): the amplitude of the $t^{-1/3}$ term goes as $\epsilon^{1/3}$, while the total contribution of the selective targets to the saturation coverage goes as ϵ. (iii) The $t^{-1/2}$ regime vanishes when ϵ increases; the $t^{-1/2}$ term has in fact an additional exponential dependence, $e^{-\epsilon^2 t}/\sqrt{t}$, which explains why for $\alpha \geqslant 1.5$ in the case of ellipses and spherocylinders ($\epsilon \geqslant 0.5$) and for squares ($\epsilon=0.414\cdots$) there is no detectable trace of $t^{-1/2}$ behavior. These results, which do not depend on the specific form of $k(h)$ given in Eq. (5), also explain why the numerical analysis of the simulation data for weakly elongated ellipses and spherocylinders ($\alpha=1.25$) does not give the $t^{-1/3}$ behavior, but rather a mixture of $t^{-1/2}$ and $t^{-1/3}$ regimes that leads to an effective exponent intermediate between 1/2 and 1/3.

The results obtained for the saturation coverage at the jamming limit are given in Tables I–III. They are also displayed in Fig. 2, together with the values already published in the literature for ellipses[18,20] and rectangles,[21] as a function of the aspect ratio. The curves obtained for the three shapes (spherocylinders, ellipses, rectangles) show a maximum and seem to go to zero when the aspect ratio becomes very large. This latter feature, as we argue in the next section, must be common to all convex bodies. On the other hand, we have no proof for the necessary presence of a maximum when the aspect ratio increases. The maximum value for spherocylinders and ellipses is obtained for $\alpha\simeq 2$ and is necessarily greater than the saturation coverage for hard disks, since both spherocylinders and ellipses reduce to disks when $\alpha\to 1$. Indeed, we find $\theta_{\max}(\infty)\simeq 0.581$ for spherocylinders and an almost identical value, $\theta_{\max}(\infty)\simeq 0.583$, for ellipses. The curve for rectangles displays a maximum at $\alpha\simeq 1.6$ and the corresponding saturation coverage, $\theta_{\max}(\infty)\simeq 0.55$, is only slightly larger than that of hard disks: for $\alpha\to 1$, rectangles reduce to squares which have a saturation coverage, $\theta_{\text{square}}\simeq 0.530$, which is notably less the hard-disk value, $\theta_{\text{disk}}\simeq 0.547$.[17] Instead of using α to measure the anisotropy, one can choose $e=1+\epsilon$, where ϵ is the parameter introduced above to discuss the filling process of selective and nonselective targets. The elongation e is thus equal to the ratio of the longest length over the width or small axis: for spherocylinders or ellipses $e=\alpha$, but for squares and rectangles $e=\sqrt{1+\alpha^2}$. A square ($\alpha=1$, $e=\sqrt{2}$) should then not be compared to a disk ($\alpha=e=1$), but to an ellipse or a spherocylinder with $\alpha=\sqrt{2}$; similarly, a rectangle of aspect ratio α "behaves" rather like an ellipse or spherocylinder of aspect ratio $\sqrt{1+\alpha^2}$. The difference between α and e is not relevant for very elongated objects, but, as shown in Fig. 3, by plotting $\theta(\infty)$ as a function of e in place of α, one observes that the location of the maximum is roughly independent of the shape: filling a surface by unoriented hard convex objects seems to be more efficient for objects with an elongation e close to 2. This will be discussed in more detail in Paper II.

IV. LIMIT OF VERY ELONGATED OBJECTS

There are two ways to approach the limit of infinitely large aspect ratios: either by letting the width l (or small axis b) go to zero while keeping the length L (or long axis a) constant, or by letting the width (small axis) go to zero while keeping the proper area constant. In the first case, the proper area goes to zero, and this corresponds to infinitely thin needles, or line segments. In the second case, the length (long axis) becomes infinite in order to maintain a nonzero proper area. The consequences for the RSA process are important: the filling of a surface by needles presents no jamming limit and the density of adsorbed needles keeps increasing (this somewhat parallels the observation that equilibrium systems of hard needles have no finite freezing density[28]). As shown by Tarjus and Viot,[23] the long-time kinetics for needles is algebraic, but the exponent is not simply related to the number of degrees of freedom per object. The reason is that there is a competition, at all times, between destruction and creation of targets which results in an irrational exponent,

$$\rho(t)\sim t^{\sqrt{2}-1}, \quad t\to+\infty, \tag{8}$$

where $\rho(t)$ is the number density of needles. Equation (8) was rigorously proved for a one-dimensional system and conjectured to be also valid for the two-dimensional system.[23] Recent extensive simulations by Ziff and Vigil[22] support this prediction.

On the other hand, there is always a jamming limit for objects with a nonzero proper area and the saturation coverage decreases as the aspect ratio increases. As pointed out by Vigil and Ziff[21] in their simulation study of unoriented rectangles, the RSA kinetics for very elongated rectangles (with a nonzero proper area) is very close to that of line segments for most times except the longest. For short and intermediate times, the rejection of trial rectangles due to overlap with preadsorbed rectangles is controlled by the largest linear size, since the probability to overlap just the widths without crossing the lengths is much smaller than the probability to adsorb in an open space. Rectangles "behave" effectively as line segments (needles). For longer times, when the ASF is very small and composed of isolated targets, the width of the rectangles becomes relevant for the rejection process and one enters the asymptotic regime described in the previous section. We will thus assume that the RSA kinetics for very elongated objects (here, the shape is not relevant) is governed by two successive regimes: an intermediate needlelike regime and the usual asymptotic regime. The initial regime corresponding to very short times (see Paper II) shrinks for very large ratios[21] and is not relevant for determining the saturation coverage.

The starting point consists in defining two pairs of scaling variables,

$$t=sN, \quad \theta_\alpha=sn, \tag{9}$$

$$t'=\alpha sN, \quad \rho'_\alpha=\alpha sn, \tag{10}$$

where N is the number of trials, n is the number of adsorbed objects, and s is the relative proper area of an object. The first pair, Eq. (9), refers to the usual scaling variables for a RSA process. The second one, Eq. (10), is appropriate for the needles: αs is simply equal to L^2 (or a^2) divided by the area of the square cell, and the variables are then well defined when $\alpha\to+\infty$ and $s\to 0$. Using the generalized Langmuir equation, Eq. (1), and defining Φ as the ASF averaged over all orientations, one can write

$$\Phi(t)=\frac{d\theta_\alpha}{dt}=\frac{d\rho'_\alpha}{dt'}. \tag{11}$$

At short and intermediate times (needlelike regime), the average ASF Φ, as obtained by combining Eq. (8) and Eq. (11), decreases as $t'^{\sqrt{2}-2}$. Further, using the one-to-one mapping between time and density and the fact that the kinetics in this regime is independent of the width of the objects gives

$$\Phi(t')\simeq c\rho'^{-\sqrt{2}}_\alpha, \tag{12}$$

where c is independent of the aspect ratio α. For long times (asymptotic regime), Φ is expressible with the help of Eqs. (4) and (8), which finally leads to

$$\Phi(t)\simeq d[\theta_\alpha(\infty)-\theta_\alpha]^4. \tag{13}$$

To proceed further, we make the two following assumptions: First, that for large aspect ratios the crossover region between the two critical regimes extends over a small range of times so that it is meaningful to define a matching point between the two regimes; and second, that the relative importance of the two regimes in the filling process stays essentially constant when α becomes infinite. If this were not the case, one regime would shrink to zero when $\alpha\to+\infty$. Both assumptions are well supported by existing simulation data.[21,22] Introducing the dimensionless variable $x=\theta_\alpha/\theta_\alpha(\infty)$ and using Eqs. (9)–(13), one obtains the following equation for the value of x at the matching point:

$$d\theta^4_\alpha(\infty)(1-x)^4=c[\alpha\theta_\alpha(\infty)x]^{-\sqrt{2}}, \tag{14}$$

which can be rewritten as

$$\alpha^{\sqrt{2}}\theta^{4+\sqrt{2}}_\alpha(\infty)=c[d(1-x)^4x^{\sqrt{2}}]^{-1}. \tag{15}$$

Since we have assumed that both regimes contribute in a comparable way to the filling process when $\alpha\to+\infty$, the value of x at the matching point and the coefficient d must not diverge nor go to zero in this limit. As a consequence, the right-hand side of Eq. (15) can be taken as independent of α, and the following asymptotic result for the saturation coverage is derived:

$$\theta_\alpha(\infty)\sim\alpha^{-1/(1+2\sqrt{2})}, \quad \alpha\to+\infty. \tag{16}$$

We thus obtain that the saturation coverage for very elongated objects with a nonzero proper area (irrespective of their shape) goes to zero when the aspect ratio α becomes infinite according to a power law, the exponent of which is equal to $-1/(1+2\sqrt{2})\simeq-0.26$. This is compatible with the behavior observed in simulations of elongated rectangles. In particular, from a log–log plot of their data, Vigil and Ziff gave a numerical estimate of the exponent equal to

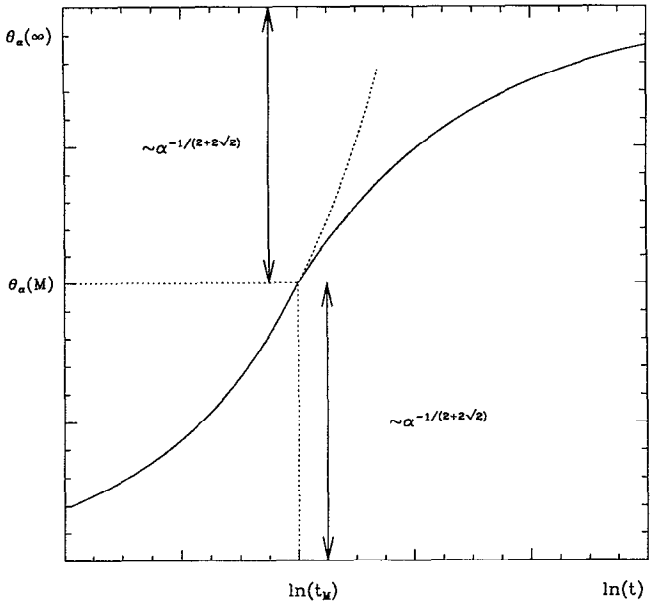

FIG. 4. Illustration of the time evolution of the coverage [θ_α vs $\ln(t)$] for a very large aspect ratio α as predicted by Eqs. (9)–(15). $\theta_\alpha(M)$ and t_M indicate, respectively, the surface coverage and the characteristic time at the matching point between the needlelike regime and the asymptotic regime.

-0.20.[21,22] Considering the difficulty of obtaining reliable data for very elongated objects and the fact that our prediction is only asymptotically valid, the agreement seems rather satisfactory.

From Eq. (16) and the definition of x, it is clear that the two regimes contribute to the saturation coverage with a comparable weight, when $\alpha \to +\infty$,

$$\theta_\alpha(\infty) - \theta_\alpha(M) \sim \theta_\alpha(M) \sim \alpha^{-1/(1+2\sqrt{2})}, \tag{17}$$

where M indicates the matching point; this is illustrated in Fig. 4. The time t_M corresponding to the crossover between the needlelike and the asymptotic regimes is obtained from Eqs. (9), (10), and (14) and goes as

$$t_M \sim \alpha^{3/(1+2\sqrt{2})}, \quad \alpha \to +\infty. \tag{18}$$

This result indicates that the asymptotic approach to the jamming limit (characterized by the $t^{-1/3}$ behavior) starts at longer and longer times when the aspect ratio increases, as is indeed observed in the computer simulation of very elongated rectangles.[21]

Finally, the asymptotic result derived for the saturation coverage of very elongated objects can be used to determine the fractal dimension of the system of adsorbed needles. According to the arguments given by Ziff and Vigil,[22] the fractal dimension may be obtained by studying how the "mass" of the ensemble of needles varies as one changes the length scale of the resolution. Looking at a configuration of needles with a resolution ϵ is equivalent to a coarse graining procedure which assigns a width ϵL to each object. By appropriately choosing the number density, the corresponding coarse grained system can be viewed as the saturation state for adsorbed rectangles of length L and width ϵL.[22] Taking the mass of the system as proportional to the saturation coverage and using Eq. (16), we then derive that the mass decreases with the resolution as $\epsilon^{1/(1+2\sqrt{2})}$ when $\epsilon \to 0$. Since for a fractal object the mass goes as ϵ^{2-D}, where D is the fractal dimension, we conclude that the fractal dimension of the system of needles is equal to $(1+4\sqrt{2})/(1+2\sqrt{2}) \simeq 1.74$.

ACKNOWLEDGMENTS

This work has been supported in part by NATO (Grant No. 890872) and NSF (Grant No. CTS-9011240). We thank Professor R. M. Ziff for drawing our attention to the issue of fractal dimension.

[1] J. Feder, J. Theor. Biol. **87**, 237 (1980).
[2] J. Feder and I. Giaever, J. Colloid Interface Sci. **78**, 144 (1980).
[3] A. Schmitt, R. Varoqui, S. Uniyal, J. L. Brash, and C. Pusiner, J. Colloid Interface Sci. **92**, 25 (1983).
[4] G. Y. Onoda and E. G. Liniger, Phys. Rev. A **33**, 715 (1986).
[5] Z. Adamczyk, M. Zembala, B. Siwek, and P. Warszyński, J. Colloid Interface Sci. **140**, 123 (1990).
[6] A. Rényi, Publ. Math. Inst. Hung. Acad. Sci. **3**, 109 (1958).
[7] B. Widom, J. Chem. Phys. **44**, 3888 (1966).
[8] J. J. Gonzáles, P. C. Hemmer, and J. S. Høye, Chem. Phys. **3**, 228 (1974).
[9] G. Tarjus, P. Schaaf, and J. Talbot, J. Stat. Phys. **63**, 167 (1991).
[10] P. Schaaf and J. Talbot, Phys. Rev. Lett. **62**, 175 (1989); J. Chem. Phys. **91**, 4401 (1989).
[11] A. Baram and D. Kutasov, J. Phys. A **22**, L251 (1989).
[12] J. W. Evans, Phys. Rev. Lett. **62**, 2642 (1989).
[13] R. Dickman, J. S. Wang, and I. Jensen, J. Chem. Phys. **94**, 8252 (1991).
[14] J. A. Given, Phys. Rev. A **45**, 816 (1992).
[15] Y. Pomeau, J. Phys. A **13**, L193 (1980).
[16] R. H. Swendsen, Phys. Rev. A **24**, 504 (1981).
[17] E. L. Hinrichsen, J. Feder, and T. Jøssang, J. Stat. Phys. **44**, 793 (1986).
[18] J. Talbot, G. Tarjus, and P. Schaaf, Phys. Rev. A **40**, 4808 (1989).
[19] P. Viot and G. Tarjus, Europhys. Lett. **13**, 295 (1990).
[20] J. D. Sherwood, J. Phys. A **23**, 2827 (1990).
[21] R. D. Vigil and R. M. Ziff, J. Chem. Phys. **93**, 8270 (1990).
[22] R. M. Ziff and R. D. Vigil, J. Phys. A **23**, 5103 (1990); R. M. Ziff (private communication).
[23] G. Tarjus and P. Viot, Phys. Rev. Lett. **67**, 1875 (1991).
[24] R. D. Vigil and R. M. Ziff, J. Chem. Phys. **91**, 2599 (1989).
[25] B. J. Brosilow, R. M. Ziff, and R. D. Vigil, Phys. Rev. A **43**, 631 (1991).
[26] M. C. Bartelt and V. Privman, Phys. Rev. A **44**, R2227 (1991).
[27] G. Tarjus and J. Talbot, Phys. Rev. A **45**, 4162 (1992).
[28] D. Frenkel and R. Eppenga, Phys. Rev. A **31**, 1776 (1985).